

Trivalent atoms defect-complexes induced defect  
levels in germanium for enhanced Ge-based device  
performance

Emmanuel Igumbor<sup>1\*</sup>, Moise Dongho-Nguimdo<sup>2†</sup>,  
Edwin Mapasha<sup>3†</sup>, Rajendran Kalimuthu<sup>4†</sup>, Abdulrafiu Raji<sup>5,6†</sup>,  
Walter Meyer<sup>3†</sup>

<sup>1</sup>Mechanical Engineering Science, University of Johannesburg,  
Johannesburg, South Africa.

<sup>2</sup>Department of Electrical and Electronic Engineering, College of  
Technology, University of Buea, Buea, P.O.Box 63, Cameroon.

<sup>3</sup>Department of Physics, University of Pretoria, Pretoria, 0002, South  
Africa.

<sup>4</sup>Department of Polymer Science, University of Madras, Guindy  
Campus, Chennai 600025, India.

<sup>5</sup>Center for Augmented Intelligence and Data Science, College of  
Science, Engineering and Technology, University of South Africa,  
Florida 1709, South Africa.

<sup>6</sup>National Institute of Theoretical and Computational Sciences  
(NITheCS), South Africa.

\*Corresponding author(s). E-mail(s): [elgumuk@gmail.com](mailto:elgumuk@gmail.com);

Contributing authors: [donghomoise@gmail.com](mailto:donghomoise@gmail.com) ;

[edwin.mapasha@up.ac.za](mailto:edwin.mapasha@up.ac.za) ; [rajendran5050@gmail.com](mailto:rajendran5050@gmail.com) ;

[tunderaji@gmail.com](mailto:tunderaji@gmail.com) ; [wmeyer@up.ac.za](mailto:wmeyer@up.ac.za);

†These authors contributed equally to this work.

001  
002  
003  
004  
005  
006  
007  
008  
009  
010  
011  
012  
013  
014  
015  
016  
017  
018  
019  
020  
021  
022  
023  
024  
025  
026  
027  
028  
029  
030  
031  
032  
033  
034  
035  
036  
037  
038  
039  
040  
041  
042  
043  
044  
045  
046

## Abstract

Defect-complexes have significant impacts on the structural, electronic, optical, and electrical properties of semiconductors. Several defect-complexes formed by the  $n$ -type and  $p$ -type atoms in Ge has been implemented for the development of improved modern microelectronic devices. However, there is no reported study on the substitution-interstitial defect-complexes formed by trivalent atoms in Ge. In this paper, the hybrid density functional theory study of the structural, electronic, formation and defect levels induced by the trivalent substitution-interstitial ( $B_{Ge}B_i$ ,  $Al_{Ge}Al_i$ ,  $Ga_{Ge}Ga_i$  and  $In_{Ge}In_i$ ) defect-complexes in Ge are presented. The formation energy results showed that the trivalent substitution-interstitial defect-complexes in Ge formed with relatively low energies. The  $Ga_{Ge}Ga_i$ , under equilibrium conditions is the most energetically favourable, with a formation energy of 3.95 eV. All trivalent atoms are bound with their respective substitution and interstitial atoms without dissociation. With respect to their ability to form as a defect cluster, the  $In_{Ge}In_i$  is the most stable defect-complex, with a binding energy of 2.91 eV. Except for the  $Ga_{Ge}Ga_i$ , all studied defect-complexes are electrically active. The  $B_{Ge}B_i$  and  $Al_{Ge}Al_i$  induced single acceptor level, while the  $In_{Ge}In_i$  induced active donor levels. The acceptor defect level induced by the  $B_{Ge}B_i$  is deep and that of the  $Al_{Ge}Al_i$  is shallow, close to the conduction band. The results of this study are important as they provide theoretical insights into the experimental characterisation of the substitution-interstitial defect-complexes formed by trivalent impurities in germanium, which could help to improve Ge-based microelectronic devices.

**Keywords:** Germanium, formation energy, binding energy, defect level, substitution-interstitial, defect-complexes, DFT

## 1 Introduction

Recent developments in nanoelectronics, optoelectronics and microelectronics have led to significant interest in the improvement of modern semiconductor technology [1, 2]. Several semiconductors including those of the Si and Ge [3] have been developed for advancement applications in microelectronics. Amongst the group IV semiconductors, Ge stands out as a gateway material for the development of semiconductor transistor [4] and fully complementary metal oxide semiconductor (CMOS). Ge has a higher low-field carrier mobilities compared to Si [3]. However, the performance of Ge-based devices may be influence by the presence of impurities such as point defects or extended defects [5].

Point defects are sometimes unintentionally introduced into their hosts during metal-organic chemical vapor deposition (MOCVD) [6] or synthesis [7–9]. For example, carbon impurity can be easily introduced into a semiconductor during MOCVD, which may act as a source of yellow luminescence [10, 11]. The ion implantation technique introduces controlled defects into crystal lattice of a material. This process involves directing high-energy ions at the crystal, causing lattice damage and the introduction of defects [12, 13]. High-energy particles, such as electrons, protons, or ions, are used to irradiate germanium crystal, leading to the formation of defects. Such defects may migrate, annihilate, or aggregate during annealing. The introduction of large isovalent dopants such as Sn can influence interactions in Ge and Si [14]. Via fabrication and defect processes, high-quality Ge-based direct band gap semiconductor can be realized [15, 16]. Trivalent atoms have been used to doped materials for the realization of *p*-type semiconductors. The trivalent impurities introduced as interstitial significantly enhance diffusion activities in Si [17]. Study revealed that the electron transport and recombination properties of SiC nanotube [18] is influenced by the presence of trivalent atoms. Doping group IV atoms (Si, Ge) with trivalent atoms boron (B), indium (In), and gallium (Ga)) increase the number of holes in Si and Ge [19]. Furthermore, the trivalent doping has been used to established the energy and spatial distribution of intrinsic hole traps in dry thermal silicon dioxide [20] as well as, used as charge compensating defects in Ge [21].

Point defects can exist in crystalline materials such as interstitials, substitutions, antisites, or vacancies. These individual point defects can combine in a material, leading to the formation of defect complexes [22, 23]. Several studies that reported the formation of defect-complexes in semiconductor, including Ge or Si have been documented [24–26]. For instance, the nitrogen substitution and vacancy-complex in SiC is a defect-complex which has been identified as a strong candidate for application in quantum technologies [27, 28]. The monovacancy defect-complexes in

139 Ge have been observed to remain thermodynamically stable, even following high-  
140 temperature annealing. The nucleation and thermal evolution of these monovacancy  
141 defect-complexes holds significant importance for the manufacturing of future Ge-  
142 based electronic devices [29]. Defect-complexes of vacancy-donor pairs in *n*-type Ge  
143 doped with As, P, and Sb have been reported [30]. While defect-complexes with fewer  
144 P atoms exhibit negative charge, the introduction of Sb into Ge creates the presence  
145 of multiple competing traps in the positron trapping process [30].  
146  
147  
148

149 To achieve a high quality Ge-based electronic device, the influence of defect-  
150 complexes in the host materials must be well understood and controlled [25, 28, 31].  
151  
152 Despite several studies that reported important results of defect-complexes in Ge,  
153 there is lack of information on the trivalent atoms substitution and interstitial defect-  
154 complexes in Ge. Furthermore, considering the applicability of Ge in modern electronic  
155 devices, it is important that a detailed study of the trivalent atoms substitution and  
156 interstitial defect-complexes be carried out to provide information of their induced  
157 defect levels and how they may be controlled during device fabrication. Herein, we  
158 present computational studies which enable the understanding of electrically active  
159 defect levels induced by trivalent atoms substitution and interstitial defect-complexes  
160 in Ge.  
161  
162  
163  
164  
165  
166  
167  
168

169 In this study, results of the various defect levels induced by the trivalent atoms  
170 substitution-interstitial defect-complexes in Ge were presented. The defect-complexes  
171 studied are  $B_{Ge}B_i$ ,  $Al_{Ge}Al_i$ ,  $Ga_{Ge}Ga_i$  and  $In_{Ge}In_i$ . Where  $B_{Ge}B_i$  is a defect-complex  
172 consisting of B atom in Ge lattice position ( $B_{Ge}$ ) and B atom in an interstitial position  
173 ( $B_i$ ). The density functional theory (DFT) calculations with the Heyd, Scuseria and  
174 Ernzerhof (HSE06) [32] hybrid functional were used to predict the most energetically  
175 favorable trivalent atoms substitution-interstitial defect-complexes and their stability  
176 in Ge. We showed that the trivalent substitution-interstitial defects in Ge are stable.  
177 Strong induced electrically active defect level were observed for the  $Al_{Ge}Al_i$ ,  $B_{Ge}B_i$   
178  
179  
180  
181  
182  
183  
184

and  $\text{In}_{\text{Ge}}\text{In}_i$ . Finally, we provided a crucial understanding of the electrical active defect levels induced by the trivalent atoms substitution-interstitial defect-complexes in Ge, which could be courted for application in improved germanium-based microelectronic devices.

## 2 Method

First-principle calculations were performed using the DFT as implemented in the Vienna *Ab-initio* Simulation Package [33, 34]. The projected augmented wave method was used to describe the core electron interactions. The  $s^2p^1$  was used as the valence electrons for the group III (trivalent) atoms and the  $s^2p^2$  was used as the valence electrons for the Ge. The HSE06 hybrid functional with the PBE of the generalized gradient approximation (GGA) was used as the exchange correlation. The HSE which is a mixture of the PBE and Hartree-Fock has been successfully used to predict accurate band gap of the semiconductors and provides an improved defect levels of various point defects in semiconductors [23, 35, 36]. This is in contrast to the local density approximation and GGA, which are known to underestimate the band gap of semiconductor materials, and hence, inadequately predict the defect levels in semiconductors [37–39]. In our calculations, we used a default mixing parameter of 25% and screening parameter of  $0.2 \text{ \AA}^{-1}$  as implemented in the HSE. It is important to point out that our choice of the HSE is guided by its capacity to accurately reproduce the experimental band gap of Ge [40]. To model the various defect-complexes in Ge, in particular, their formation, electrical and electronic properties, we constructed a supercell of size  $2 \times 2 \times 2$  which has 64 atoms. The supercell is then optimized using the conjugate gradient algorithm with an atomic force convergence criterion lower than  $0.01 \text{ eV/\AA}$ . We integrated the Brillouin zone using the Monkhorst-Pack scheme with a grid of  $2 \times 2 \times 2$   $\mathbf{k}$ -points for both the pristine and defective supercell. However, we used a denser  $\mathbf{k}$ -point grid of  $20 \times 20 \times 20$  to calculate the density of states.

231 The well converged energy cut-off of 400 eV has been previously used to model the  
 232 electronic and defect properties of impurities in Ge, and consequently produce results  
 233 that are consistent with experimental data [41]. Thus, in this study, the energy cut-off  
 234 for all the calculations was set to 400 eV, and the minimum total energy difference  
 235 convergence criteria was set to below  $10^{-5}$  eV.

239 The formation energy ( $E^F(\text{defect} - \text{complex}, q)$ ) of a defect-complex in its charge  
 240 state  $q$  as a function of the Fermi energy ( $\varepsilon_F$ ) is defined as

$$\begin{aligned}
 241 & \\
 242 & \\
 243 & \\
 244 & E^F(\text{defect} - \text{complex}, q) = E(\text{defect} - \text{complex}, q) - E(\text{pristine}) \\
 245 & \\
 246 & \quad + \sum_i \Delta(n)_i \mu_i + q[E_V + \varepsilon_F] + E_{FNV}^q, \\
 247 & \\
 248 & \\
 249 & \\
 250 & \\
 251 & \\
 252 & \\
 253 & \\
 254 & \\
 255 & \\
 256 & \\
 257 & \\
 258 & \\
 259 & \\
 260 & \\
 261 & \\
 262 & \\
 263 & \\
 264 & \\
 265 & \\
 266 & \\
 267 & \\
 268 & \\
 269 & \\
 270 & \\
 271 & \\
 272 & \\
 273 & \\
 274 & \\
 275 & \\
 276 &
 \end{aligned}
 \tag{1}$$

249 where the  $E(\text{defect} - \text{complex}, q)$  is the total energy of the supercell with a defect,  
 250 the  $E(\text{pristine})$  is the total energy of the pristine supercell. The chemical potential  
 251 of the  $i$ th-type atom which represents the Gibbs free energy when an isolated atom  
 252 exchange with the heat reservoir is represented as  $\mu$ . The  $n$  is the number of atoms  
 253 that are added or removed from the defective supercell. The chemical potentials of  
 254 the trivalent atoms were calculated as the total energy per number of impurity atoms.  
 255 The  $E_V$  is the energy of the valence band maximum (VBM). The  $E_{FNV}^q$  according to  
 256 Freysoldt, Neugebauer and Van de Walle method [42] is the energy correction term,  
 257 which accounts for the errors due to the finite size of the supercell and defect-defect  
 258 interactions problems.

266 Defect level is described from the charge state transition energies. The energy  
 267 needed for an atom or ion to change from one charged state to another is the charge  
 268 state transition energy level [5]. A neutral atom can gain or lose electrons to change its  
 269 charge from being positively charged to negatively charged. The transition of electrons  
 270 between various energy levels within an atom occurs when an atom's charge state  
 271 changes. To theoretically determine the positions of defect levels in the semiconductor

band gap, the width of the band gap must be known. For the pure Ge crystal, the band gap of 0.78 eV were previously obtained using the hybrid density functional [43], which agrees with experimental results of 0.78 eV as reported in Ref. [40]. The charge state transition energy level ( $\epsilon(q/q')$ ) is the Fermi energy for which two charge states ( $q$  and  $q'$ ) in the band gap have the same energy. This is calculated as

$$\epsilon(q/q') = \frac{E^F(\text{defect} - \text{complex}, q) - E^F(\text{defect} - \text{complex}, q')}{q' - q}, \quad (2)$$

where the  $E^F(\text{defect} - \text{complex}, q)$  and  $E^F(\text{defect} - \text{complex}, q')$  are calculated at  $\epsilon_F = 0$ . In this study, the considered charge states ( $q$ ) are -2, -1, 0, +1 and +2. Other charge states were not included as they are thermodynamically unstable.

The possibility of a defect-complex to disassociate into non-interacting defects under equilibrium conditions [23] needs to be understood. Hence, to provide information whether a defect-complex is energetically stable, it is imperative that the binding energy of such defect should be known. The binding energy is defined as the energy required to split a defect-complex into a non-interacting defect. In this study, the binding energy of a defect-complex is calculated using Eq. 3.

$$E_b = E_{\text{interstitial}}^F + E_{\text{substitution}}^F - E_{\text{defect-complex}}^F, \quad (3)$$

where  $E_{\text{interstitial}}^F$ ,  $E_{\text{substitution}}^F$  and  $E_{\text{defect-complex}}^F$  are the formation energies of the interstitial, substitution and defect-complex of trivalent impurities in Ge, respectively. From Eq. 3, negative binding energy implies that a defect cluster formation is energetically unfavorable with respect to its constituent isolated components. Thus, the defect-complex is liable to dissociate with an amount of energy lower than its formation energy.

### 323 **3 Results and discussion**

324

325 In this section, results of the structural and electronic properties, formation and sta-  
326 bility of defect-complexes as well as the thermodynamically charge state transition  
327 levels in Ge were presented.  
328

329  
330 In a crystalline solid structure, the location and distribution of defects may be ran-  
331 dom. Therefore, when modeling defects in a solid crystal structure, it is important to  
332 take into consideration the various possible defect sites in order to obtain the most  
333 energetically favorable defect configurations. In this study, we adopted the method  
334 used by Igumbor *et al* [41] to ascertain the most energetically defect-complex config-  
335 uration. According to Ref. [41], two different defect configurations were considered:  
336 these are when both the substitution and interstitial atoms are (i) nearest neighbour;  
337 and (ii) not nearest neighbour. Igumbor *et al* [41] showed that both configurations  
338 (i) and (ii) are energetically favorable with relatively low formation energies. How-  
339 ever, the substitution and interstitial atoms as nearest neighbour defect-complex was  
340 more energetically favorable. Hence, in this present study, we focused only on the  
341 defect-complex configuration where the substitution and interstitial atoms are nearest  
342 neighbor.  
343  
344  
345  
346  
347  
348  
349  
350  
351

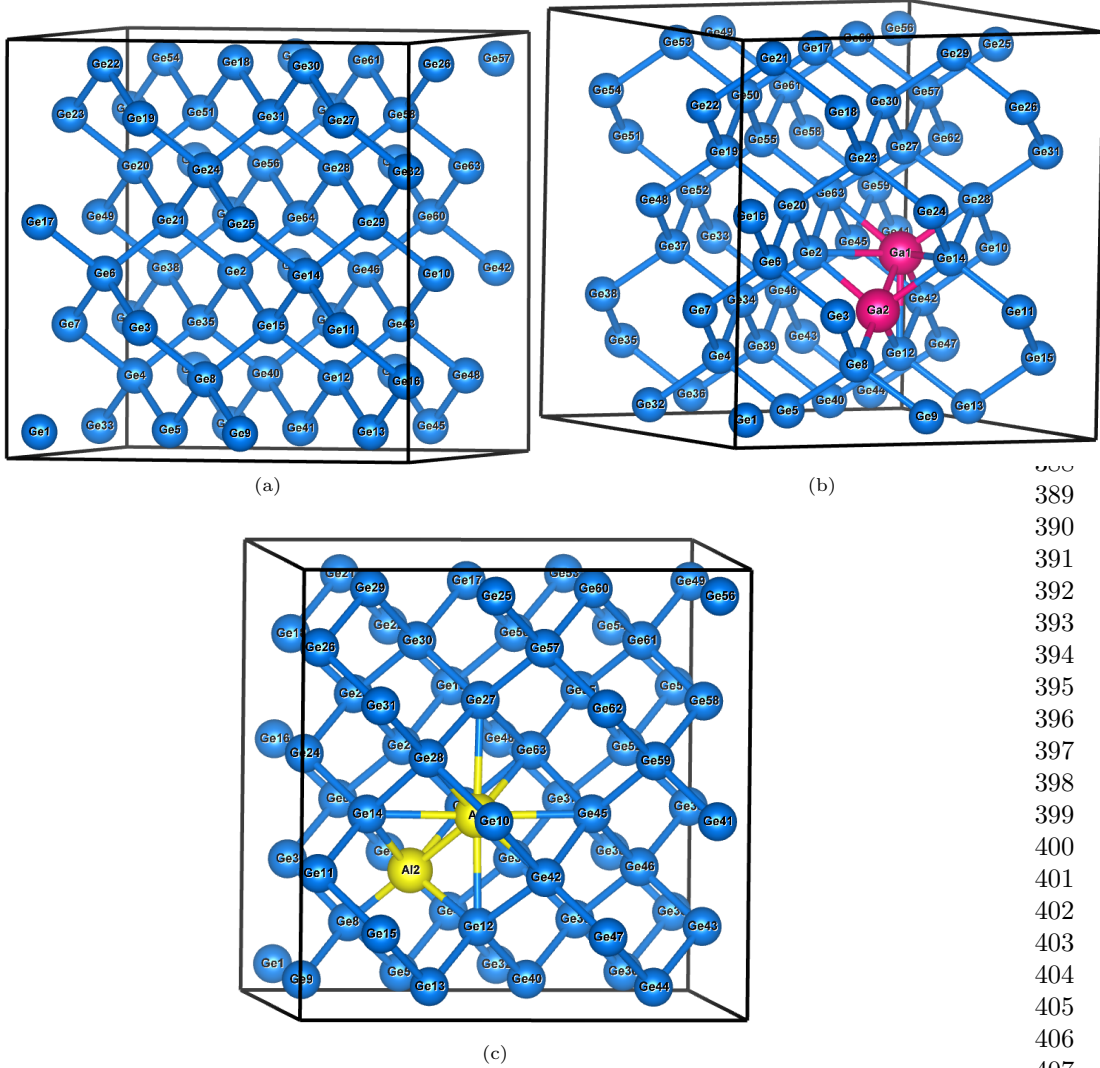
#### 352 **3.1 Structural properties**

353

354 Fig. 1 shows the relaxed geometric structure of pristine Ge,  $\text{Ga}_{\text{Ge}}\text{Ga}_i$ , and  $\text{Al}_{\text{Ge}}\text{Al}_i$ .  
355 Table 1 shows the various relaxed bond lengths of the impurity and Ge atoms for  
356 the defect-complexes. The bond lengths of the  $X_{\text{Ge}}\text{-Ge}$  for all impurity atoms are  
357 shorter than that of the  $X_i\text{-Ge}$ . Except for the B-Ge, all the  $X_i\text{-Ge}$  bond distances  
358 are higher than the relaxed pristine Ge-Ge bond length. The various impurity atoms  
359 experienced different levels of strain in their bond lengths. The relaxed bond length of  
360 the  $X_{\text{Ge}}\text{-Ge}$  namely: B-Ge, Al-Ge, Ga-Ge and In-Ge are 0.51, 0.06, 0.07 and 0.02 Å,  
361 respectively, which are different from that of the pristine Ge-Ge. This suggests that  
362  
363  
364  
365  
366  
367  
368

there is significant strain induced in the system, which could influence the amount of energy required for such defects to form in Ge.

369  
370  
371  
372  
373



388  
389  
390  
391  
392  
393  
394  
395  
396  
397  
398  
399  
400  
401  
402  
403  
404  
405  
406

**Fig. 1** Relaxed geometric structure of (a) pristine Ge, (b)  $\text{Ga}_{\text{Ge}}\text{Ga}_i$ , and (c)  $\text{Al}_{\text{Ge}}\text{Al}_i$ .

407  
408  
409  
410  
411  
412  
413  
414

We also evaluated the bond order to ascertain whether a bond is formed between the defective atoms, as well as the host. A bond order of 1.34 was found between the two B atoms. This is an indication that the two B atoms are strongly bound to each

415  
416  
417  
418  
419  
420  
421  
422  
423  
424  
425  
426  
427  
428  
429  
430  
431  
432  
433  
434  
435  
436  
437  
438  
439  
440  
441  
442  
443  
444  
445  
446  
447  
448  
449  
450  
451  
452  
453  
454  
455  
456  
457  
458  
459  
460

**Table 1** The bond length of the trivalent interstitial ( $X_i$ ) and substitution ( $X_{Ge}$ ) atoms with their nearest neighbor Ge atoms. The trivalent-trivalent (X-X) atomic bond length is also listed. The radii of the impurity atoms used for this study are Al=1.84 Å, B= 0.85 Å, In=1.93 Å, and Ga=1.87 Å

|       | X-X<br>(Å) | $X_{Ge}$ -Ge<br>(Å) | $X_i$<br>(Å) |
|-------|------------|---------------------|--------------|
| B-B   | 1.54       | B-Ge                | 1.95         |
| Al-Al | 2.56       | Al-Ge               | 2.40         |
| Ga-Ga | 2.51       | Ga-Ge               | 2.53         |
| In-In | 2.71       | In-Ge               | 2.48         |

other. The substitution B atom slightly shifted from its relaxed position to forming three bonds with its nearest neighbor three Ge atoms. In contrast, the B interstitial atom is strongly bound to one Ge atom. For the other defective systems, that is the  $Al_{Ge}Al_i$ ,  $Ga_{Ge}Ga_i$ , and  $In_{Ge}In_i$ , we found bond order of 0.39, 0.43, and 0.48 for Al-Al, Ga-Ga, and In-In, respectively, between the substitution-interstitial atoms. The substitution atoms are more likely to form bonds with the host Ge atoms than their interstitial counterparts.

### 3.2 Electronic properties: partial density of states

To comprehend the impact of trivalent defect-complexes on the electronic structure of Ge, we obtained the partial density of states (PDOS) as depicted in Fig. 2. In contrast to Fig. 2a, the  $B_{Ge}B_i$  induced notable orbital ground states in the band gap of Ge as shown in Fig. 2b. While the  $p$ -orbital of the B atom is predominantly visible in the conduction band minimum (CBM), the  $p$ -orbital of the Ge atom is predominantly observed at the VBM. In addition, the sharp peak from the  $s$ -orbital of the B atom contributed to the orbital ground states near the VBM. For the  $Al_{Ge}Al_i$  as shown in Fig. 2c, we observed a different pattern from that of the  $B_{Ge}B_i$ . The  $s$ -orbital of the Al atom generated a peak near the Fermi level, mainly dominated by the Al atom's  $s$ -orbital. Other defects that induced sharp peak close to the Fermi level

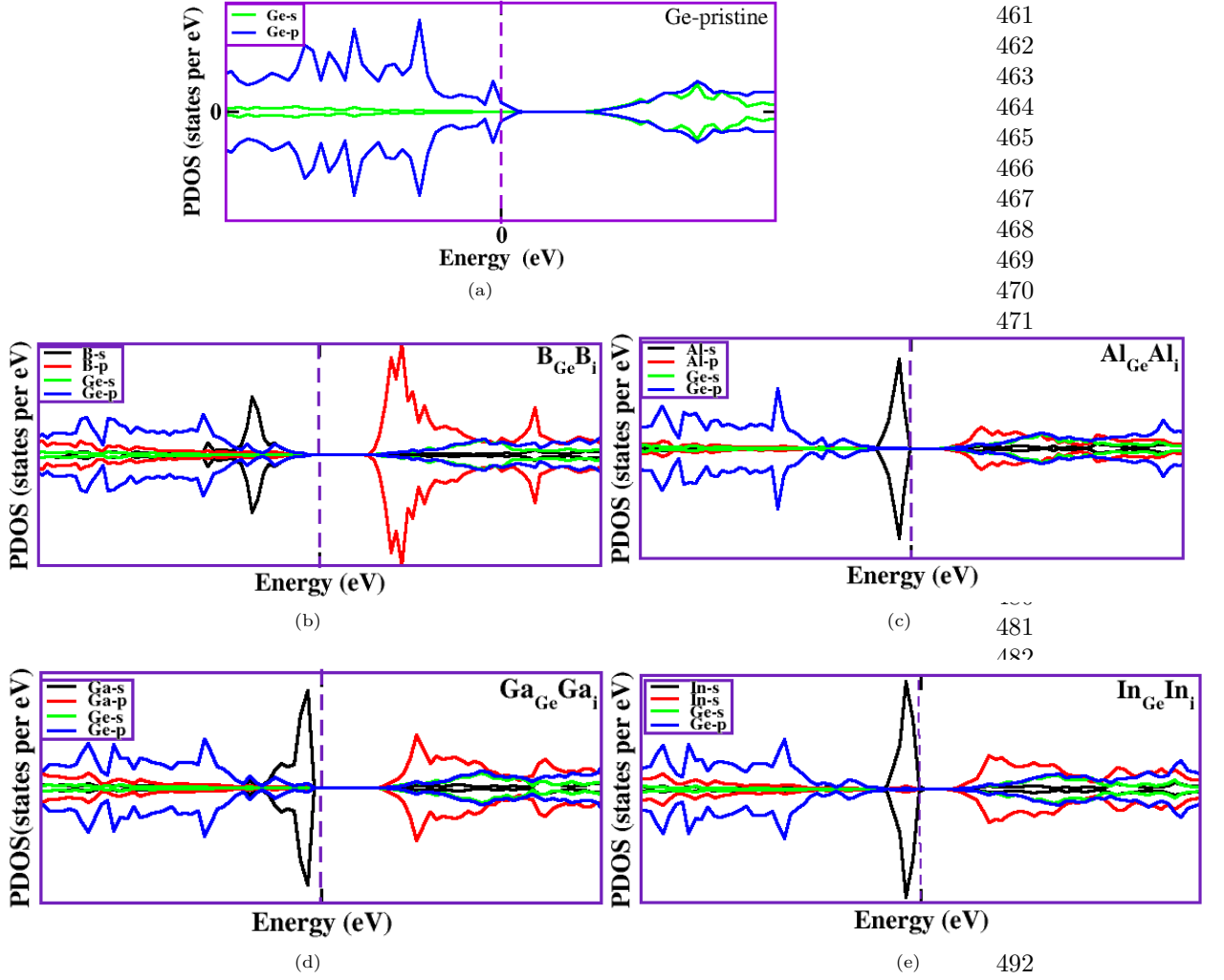


**Fig. 2** Plots of partial density of states (PDOS) of the trivalent atom substitution-interstitial defect-complexes in Ge: (a) pristine Ge; (b)  $B_{Ge}B_i$ ; (c)  $Al_{Ge}Al_i$ ; (d)  $Ga_{Ge}Ga_i$  and (e)  $In_{Ge}In_i$ . The Fermi level is set to zero and is represented by the dash line.

are the  $Ga_{Ge}Ga_i$  (Fig. 2d) and  $In_{Ge}In_i$  (Fig. 2e). In all, the positions of the Fermi-level for the defective systems are the same as that of the pristine Ge, however, the energy levels of induced orbital states differed from each defective system. For all the defective systems significant contribution of the peaks in the uppermost conduction band comes from the  $p$ -orbitals of the impurity and Ge atoms. The valence band of the defective systems are highly populated by the  $s$ -orbital of the respective impurity

507 atoms. Obvious overlapping of  $p$ -orbital of Ge/Al atoms for the  $\text{Al}_{\text{Ge}}\text{Al}_i$ , Ge/Ga atoms  
508 for the  $\text{Ga}_{\text{Ge}}\text{Ga}_i$  and Ge/In atoms of the  $\text{In}_{\text{Ge}}\text{In}_i$  were observed.  
509

510 The above observation indicates the presence of strong orbital hybridization  
511 between the  $p$ -orbital of the host and impurity atoms. Succinctly speaking, all the  
512 defects considered exhibit a  $p$ -type semiconducting characteristic and their Fermi lev-  
513 els are situated close to the valence band. Therefore, the majority carriers are mainly  
514 hole. The majority and minority spins are symmetrically aligned suggesting lack of  
515 spin polarisation. Hence, such defects in Ge may not be courted for device applications  
516 where spin dependent is required.  
517  
518  
519  
520  
521

### 522 523 **3.3 Formation energies of defect-complexes**

524 The formation energies of point defects are crucial in determining the energetics and  
525 stability of defects [5]. Fig. 3 displays the formation energies of the neutral charge state  
526 of the trivalent interstitial-substitution defect-complexes in Ge. The  $\text{B}_{\text{Ge}}\text{B}_i$ ,  $\text{Al}_{\text{Ge}}\text{Al}_i$ ,  
527  $\text{Ga}_{\text{Ge}}\text{Ga}_i$  and  $\text{In}_{\text{Ge}}\text{In}_i$ , under equilibrium conditions were energetically favorable. How-  
528 ever, the most energetically favorable is the  $\text{Ga}_{\text{Ge}}\text{Ga}_i$  with formation energy of 3.95 eV.  
529 The above results is relatively lower than di-interstitial of Ge which has a formation  
530 energy of 6.52 eV [43] for its most energetically favorable configuration. The  $\text{B}_{\text{Ge}}\text{B}_i$  is  
531 the least energetically favorable with a relatively higher formation energy of 7.39 eV.  
532 The ordering of the formation energy is therefore  $\text{B}_{\text{Ge}}\text{B}_i > \text{In}_{\text{Ge}}\text{In}_i > \text{Al}_{\text{Ge}}\text{Al}_i > \text{Ga}_{\text{Ge}}\text{Ga}_i$ .  
533 The impurity atoms used for this study have different radii ( $\text{Al}=1.84 \text{ \AA}$ ,  $\text{B}= 0.85 \text{ \AA}$ ,  
534  $\text{In}=1.93 \text{ \AA}$ ,  $\text{Ga}=1.87 \text{ \AA}$ ) [44]. Therefore, when different sizes of the participating triva-  
535 lent atoms are introduced into a pristine Ge supercell, we expect a distortion in the  
536 volume of the pure Ge crystal structure. This alteration can give rise to considerable  
537 amount of strain induced in the lattice as experienced by the bond length formed by  
538 the impurity and the nearest neighbor Ge atoms. The extent of strain experienced in  
539 the bond length could influence the formation energies required for a defect-complex  
540  
541  
542  
543  
544  
545  
546  
547  
548  
549  
550  
551  
552

to form. For instance, defect complexes involving the Al ( $\text{Al}_{\text{Ge}}\text{Al}_i$ ) and Ga ( $\text{Ga}_{\text{Ge}}\text{Ga}_i$ ),  
 formed with a relatively lower formation energies.

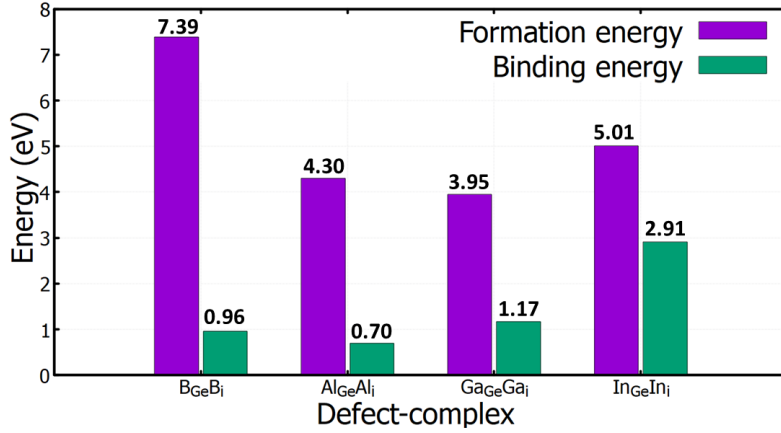


**Fig. 3** The energy of formation and the binding energy in eV of the trivalent atoms substitution-interstitial defect-complexes in Ge at  $\epsilon_{\text{F}} = 0$ .

### 3.4 Binding energies of defect-complexes

The binding energy provides information about the stability of defect-complexes relative to their constituents [5]. To ascertain if the defect-complex will dissociate into non-interacting constituents, we calculated the binding energies of the trivalent atoms defect-complexes in Ge. As shown in Fig 3, all the trivalent impurities are stable due to their positive binding energies. This suggests that the substitution and interstitial of the B, Al, Ga and In atoms bound with Ge atom as complexes. Therefore, for the defect-complex  $\text{Ga}_{\text{Ge}}\text{Ga}_i$  to dissociate into a non-interacting  $\text{Ga}_{\text{Ge}}$  or  $\text{Ga}_i$ , it will require an energy at least higher than 5.12 eV; and this can only happen if external energy of similar amount is applied to the Ge bulk containing the defect-complex. The most stable defect-complex is the  $\text{In}_{\text{Ge}}\text{In}_i$  with a binding energy of 2.91 eV. Despite the high diffusion rate of B interstitial in semiconductors [45], the  $\text{B}_{\text{Ge}}\text{B}_i$  with a high formation energy is relatively stable with a binding energy of 0.96 eV. The least energetically stable defect-complex is the  $\text{Al}_{\text{Ge}}\text{Al}_i$ . While the binding energy of the B atoms

599 pair is higher than that of Al atom pair by 0.26 eV, the binding energy of the  $\text{In}_{\text{Ge}}\text{In}_i$   
600 is higher than that of the  $\text{Ga}_{\text{Ge}}\text{Ga}_i$  by 1.74 eV. Our results show that the stability  
601 of trivalent defect-complexes increases with respect to the increasing atomic radius of  
602 the participating atoms. Based on Eq. 3, at the ambient temperature, separating the  
603 defect-complexes into their isolated non integrating defects will occur at the expense  
604 of an external perturbation of similar energy value.  
605  
606  
607  
608

609

### 610 3.5 Defect levels induced by defect-complexes

611

612 The theoretical prediction of active defect levels induced in the band gap is paramount  
613 to the identification of the electrical characteristics of defect-complexes [5]. Thus, the  
614 electrical characteristics, in particular the electrically active defect levels induced in  
615 Ge is essentially obtained from the charge state transition energy levels between the  
616 VBM and CBM [5]. For us to investigate the electrically active defect levels induced  
617 in the band gap of Ge by the substitutional-interstitial defect-complex of trivalent  
618 atoms, we plotted the graph of the formation energy as a function of the Fermi level  
619 as displayed in Fig. 4. Table 2 lists the charge state transition energy levels above  
620 the VBM. The  $\text{Ga}_{\text{Ge}}\text{Ga}_i$  is not electrically active as the neutral charge state spreads  
621 across the band gap of Ge when the Fermi energy is varied from the VBM to the  
622 CBM. While the  $\text{Al}_{\text{Ge}}\text{Al}_i$  and the  $\text{B}_{\text{Ge}}\text{B}_i$  induced a single acceptor defect level, the  
623  $\text{B}_{\text{Ge}}\text{B}_i$  induced defect level is a single deep acceptor level with an energy of  $E_C-0.21$  eV  
624 ( $E_C$  is the energy of the CBM). The  $\text{B}_{\text{Ge}}\text{B}_i$  neutral charge state spread across the  
625 band gap as the Fermi energy is varied up to 0.57 eV. The  $\text{Al}_{\text{Ge}}\text{Al}_i$  on the other  
626 hand, induced a single shallow acceptor level ( $E_C-0.02$  eV), which is very close to the  
627 CBM. The proximity of the (0/-1) to the CBM of AlGeAl<sub>i</sub> suggests that future exper-  
628 imental characterization of the defect should be conducted to confirm the existence  
629 of the induced defect level under ambient conditions, including increasing tempera-  
630 tures. Under equilibrium conditions, the (0/-1) charge state transition energy levels  
631  
632  
633  
634  
635  
636  
637  
638  
639  
640  
641  
642  
643  
644

**Table 2** The charge state transition ( $\varepsilon(q/q')$ ) defect energy levels induced by the trivalent substitution-interstitial defect-complexes in Ge. The values displayed are in eV and above the VBM.

| Defect                           | (+2/+1) | (+1/0) | (0/-1) |
|----------------------------------|---------|--------|--------|
| B <sub>Ge</sub> B <sub>i</sub>   | -       | -      | 0.57   |
| Al <sub>Ge</sub> Al <sub>i</sub> | 0.11    | 0.32   | 0.76   |
| Ga <sub>Ge</sub> Ga <sub>i</sub> | -       | -      | -      |
| In <sub>Ge</sub> In <sub>i</sub> | 0.29    | 0.57   | -      |

of the Al<sub>Ge</sub>Al<sub>i</sub> and B<sub>Ge</sub>B<sub>i</sub> can ionized at relatively energy lower than  $3 k_B T$  ( $k_B$  is the Boltzmann constant). The substitutional-interstitial defect-complex that induced donor levels are the Al<sub>Ge</sub>Al<sub>i</sub> and In<sub>Ge</sub>In<sub>i</sub>. Both defects induced single and double donor levels. The +2 charge state of the Al<sub>Ge</sub>Al<sub>i</sub> is more stable and close to the VBM, however, as the Fermi energy is varied towards the CBM, at energy of 0.32 eV, the +1 charge state becomes more thermodynamically stable. For the Al<sub>Ge</sub>Al<sub>i</sub>, the neutral charge state spreads almost 50% of the band gap. However, its (+2/+1) and (+1/0) change state transition defect levels are shallow and deep, respectively. The Al<sub>Ge</sub>Al<sub>i</sub> (+2/+1) energy level is  $E_V+0.11$  eV and that of the (+1/0) is  $E_V+0.32$  eV. The origin of compensation centre as a result of radiative and non-radiative recombination centres in semiconductor materials is linked to the activities of defect levels induced in the host. The deep defect levels induced by the Al<sub>Ge</sub>Al<sub>i</sub> are expected to decrease the radiative efficiency of Ge-based devices via recombination of excess electron-hole pairs [46]. For the In<sub>Ge</sub>In<sub>i</sub>, the energy level of the (+2/+1) is  $E_V+0.29$  whereas that of the (+1/0) is  $E_V+0.57$ . The +2 and +1 charge states spread across 70% of the band gap from the VBM. The In<sub>Ge</sub>In<sub>i</sub> deep defect levels ((+1/0) and (+2/+1) ) may not have significant effect on the transport properties of carriers. However, they can act as recombination centers for electrons and holes. Consequently, the lifetime of non-equilibrium carriers is reduced. For the (+1/0) of the Al<sub>Ge</sub>Al<sub>i</sub>, the (+1/0) and (+2/+1) of the In<sub>Ge</sub>In<sub>i</sub> increase in the concentration of electrons (holes) leads to an increase in the recombination rate. Therefore, the electrons (holes) are captured and

645  
646  
647  
648  
649  
650  
651  
652  
653  
654  
655  
656  
657  
658  
659  
660  
661  
662  
663  
664  
665  
666  
667  
668  
669  
670  
671  
672  
673  
674  
675  
676  
677  
678  
679  
680  
681  
682  
683  
684  
685  
686  
687  
688  
689  
690

691  
692  
693  
694  
695  
696  
697  
698  
699  
700  
701  
702  
703  
704  
705  
706  
707  
708  
709  
710  
711  
712  
713  
714  
715  
716  
717  
718  
719  
720  
721  
722  
723  
724  
725  
726  
727  
728  
729  
730  
731  
732  
733  
734  
735  
736

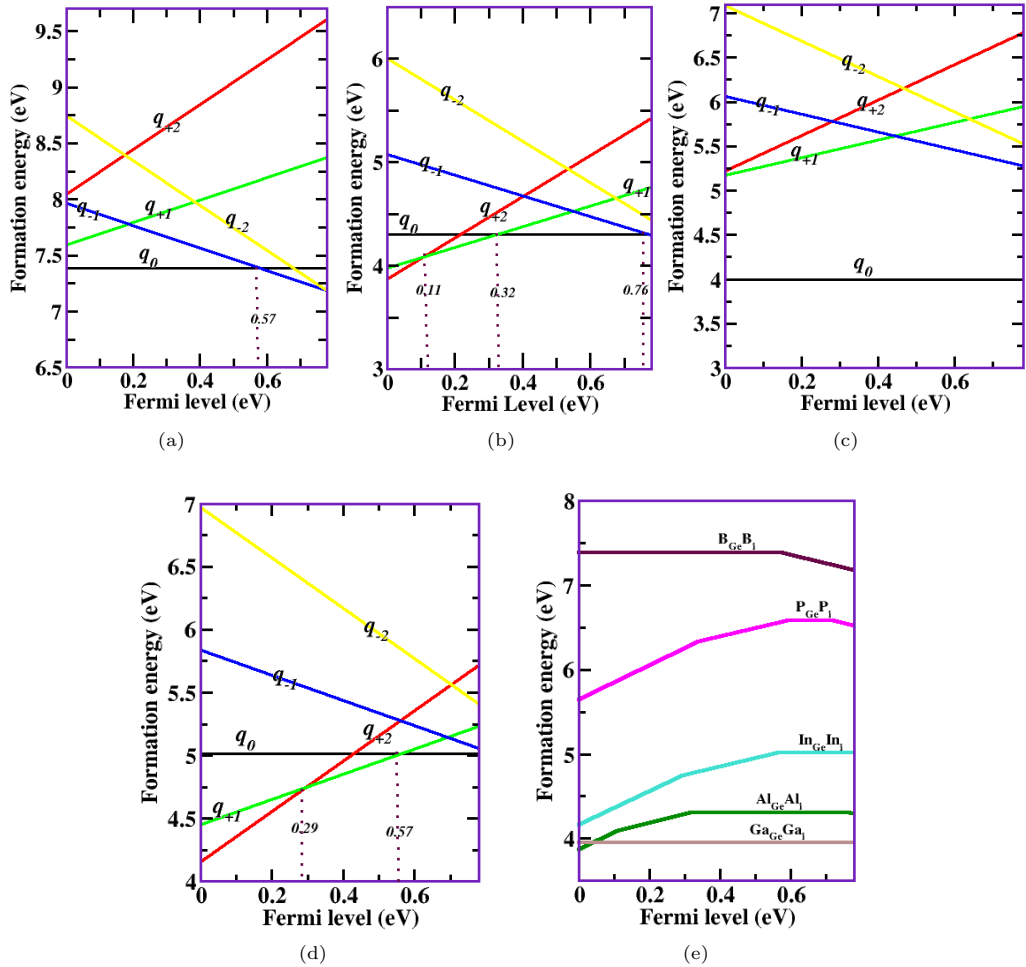


**Fig. 4** Plot of formation energy as a function of the Fermi energy for the substitution-interstitial defect-complexes formed by the trivalent atoms in Ge: (a)  $B_{Ge}B_i$ ; (b)  $Al_{Ge}Al_i$ ; (c)  $Ga_{Ge}Ga_i$ ; (d)  $In_{Ge}In_i$ ; and (e) short representation of all the possible thermodynamic charge states transition levels. The slope of each graph corresponds to the different charge states ( $q_{-2}$ ,  $q_{-1}$ ,  $q_0$ ,  $q_{+1}$  and  $q_{+2}$ ). The dash vertical line represents the possible thermodynamic stable transition energy levels.

recombined with the holes (electrons), which reduces the lifetime carriers. Finally, this study's results show that defect-complexes are important, as they revealed how their formation in Ge could influence the electrical, electronic properties and the overall performance of Ge-based devices.

## 4 Conclusion

Density functional theory calculations using hybrid functionals were conducted to determine the formation energies, stability of defect-complexes, and the electrically active defect levels induced by trivalent substitution-interstitial pairs in Ge. Under equilibrium conditions, while the  $\text{Ga}_{\text{Ge}}\text{Ga}_i$  is the most energetically favourable (energy of 3.95 eV) for the neutral charge state, the  $\text{B}_{\text{Ge}}\text{B}_i$  is the least energetically favorable with a formation energy of 7.39 eV. The ability for the defect-complexes to form as a cluster of defects was established by calculating the binding energy. All the defect-complexes reported in this study are stable with respect to their isolated defects constituting each of the defect complexes. The electronic structure results predict that the trivalent defect-complexes behave as *p*-type semiconductors. The electrically active defect levels were established from the defect levels induced in the band gap of Ge. The  $\text{Al}_{\text{Ge}}\text{Al}_i$ ,  $\text{B}_{\text{Ge}}\text{B}_i$ ,  $\text{In}_{\text{Ge}}\text{In}_i$  are all electrically active, with noticeable induced defect levels in the band gap of Ge. Whereas the  $\text{Al}_{\text{Ge}}\text{Al}_i$  and  $\text{In}_{\text{Ge}}\text{In}_i$  induced single and double donor levels, the  $\text{B}_{\text{Ge}}\text{B}_i$  induced a deep defect level. In addition, the  $\text{Al}_{\text{Ge}}\text{Al}_i$  induced a shallow acceptor level close for the CBM. The result of this study provides useful theoretical insight into the formation and stability of defects complexes that may enable the application of Ge-based materials for important electronics applications.

**Acknowledgments.** This work is based on the research supported partly by National Research foundation (NRF) of South Africa (Grant specific unique reference number 98961). The opinions, findings and conclusion expressed are those of the authors and the NRF accepts no liability whatsoever in this regard. Emmanuel Igumbor is grateful to the University of Johannesburg for funding and the Center for High Performance Computing (CHPC) Cape Town for providing computational resources.

737  
738  
739  
740  
741  
742  
743  
744  
745  
746  
747  
748  
749  
750  
751  
752  
753  
754  
755  
756  
757  
758  
759  
760  
761  
762  
763  
764  
765  
766  
767  
768  
769  
770  
771  
772  
773  
774  
775  
776  
777  
778  
779  
780  
781  
782

783 **Declarations**

784

785

786

Conflict of Interest: The authors declare that they have no conflict of interest.

787

788

789

**References**

790

791

792

793

794

- [1] P. Rajesh, Some studies on the metallic ion implanted semiconductors and their possible applications. Ph.D. thesis, Jadavpur University (2015)

795

796

797

798

799

800

801

802

803

804

805

806

807

808

809

810

811

812

813

814

815

816

817

818

819

820

821

822

823

824

825

826

827

828

- [2] W.A. Jabbara, A. Mahmood, J. Sultan, Modeling and characterization of optimal nano-scale channel dimensions for fin field effect transistor based on constituent semiconductor materials. TELKOMNIKA (Telecommunication Computing Electronics and Control) **20**(1), 221–234 (2022)
- [3] J. Yang, K. Liu, X. Chen, D. Shen, Recent advances in optoelectronic and microelectronic devices based on ultrawide-bandgap semiconductors. Progress in Quantum Electronics **83**, 100397 (2022)
- [4] S. Chander, S.K. Sinha, R. Chaudhary, A. Singh, Ge-source based l-shaped tunnel field effect transistor for low power switching application. Silicon pp. 1–14 (2021)
- [5] E. Igumbor, Hybrid functional study of point defects in germanium. Ph.D. thesis, University of Pretoria (2017)
- [6] N. Tillner, C. Frankerl, F. Nippert, M.J. Davies, C. Brandl, R. Lösing, M. Mandl, H.J. Lugauer, R. Zeisel, A. Hoffmann, A. Waag, Point defect-induced uv-c absorption in aluminum nitride epitaxial layers grown on sapphire substrates by metal-organic chemical vapor deposition. physica status solidi (b) **257**(12), 2000278 (2020)
- [7] E. Ekimov, M. Kondrin, V. Krivobok, A. Khomich, I. Vlasov, R. Khmelniyskiy, T. Iwasaki, M. Hatano, Effect of si, ge and sn dopant elements on structure

- and photoluminescence of nano-and microdiamonds synthesized from organic compounds. *Diamond and Related Materials* **93**, 75–83 (2019)
- [8] A. Bolshakov, V. Fedorov, K.Y. Shugurov, A. Mozharov, G. Sapunov, I. Shtrom, M. Mukhin, A. Uvarov, G. Cirilin, I. Mukhin, Effects of the surface preparation and buffer layer on the morphology, electronic and optical properties of the gan nanowires on si. *Nanotechnology* **30**(39), 395602 (2019)
- [9] V.E. Gora, F.D. Auret, H.T. Danga, S.M. Tunhuma, C. Nyamhere, E. Igumbor, A. Chawanda, Barrier height inhomogeneities on pd/n-4h-sic schottky diodes in a wide temperature range. *Materials Science and Engineering: B* **247**, 114370 (2019)
- [10] J. Lyons, A. Janotti, C. Van de Walle, Carbon impurities and the yellow luminescence in gan. *Applied Physics Letters* **97**(15), 152108 (2010)
- [11] A. Hernandez, M.M. Islam, P. Saddatkia, C. Coddling, P. Dulal, S. Agarwal, A. Janover, S. Novak, M. Huang, T. Dang, M. Snure, Mocvd growth and characterization of conductive homoepitaxial si-doped ga<sub>2</sub>o<sub>3</sub>. *Results in Physics* **25**, 104167 (2021)
- [12] A.E. Rugar, H. Lu, C. Dory, S. Sun, P.J. McQuade, Z.X. Shen, N.A. Melosh, J. Vuckovic, Generation of tin-vacancy centers in diamond via shallow ion implantation and subsequent diamond overgrowth. *Nano letters* **20**(3), 1614–1619 (2020)
- [13] E.A. Anber, D. Foley, A.C. Lang, J. Nathaniel, J.L. Hart, M.J. Tadjer, K.D. Hobart, S. Pearton, M.L. Taheri, Structural transition and recovery of ge implanted  $\beta$ -ga<sub>2</sub>o<sub>3</sub>. *Applied Physics Letters* **117**(15) (2020)

- 875 [14] S.R. Christopoulos, E. Sgourou, R. Vovk, A. Chroneos, C. Londos, Isovalent dop-  
876 ing and the c i o i defect in germanium. *Journal of Materials Science: Materials*  
877 *in Electronics* **29**(5), 4261–4265 (2018)  
878  
879  
880  
881 [15] M. El Kurdi, M. Prost, A. Ghrib, S. Sauvage, X. Checoury, G. Beaudoin, I. Sagnes,  
882 G. Picardi, R. Ossikovski, P. Boucaud, Direct band gap germanium microdisks  
883 obtained with silicon nitride stressor layers. *ACS photonics* **3**(3), 443–448 (2016)  
884  
885  
886 [16] Q. Wei, J. Song, C. Zhou, W. Bao, Y. Miao, H. Hu, H. Zhang, B. Wang, Study of  
887 energy band modulation of ge-based material system for monolithic optoelectronic  
888 integration chips. *Materials Express* **7**(5), 369–379 (2017)  
889  
890  
891  
892 [17] U. Södervall, M. Friesel, A. Lodding, Atomic transport of trivalent impurities  
893 in silicon: diffusion, isotope effects, activation volumes. *Journal of the Chemical*  
894 *Society, Faraday Transactions* **86**(8), 1293–1298 (1990)  
895  
896  
897  
898 [18] P. Gong, Y.J. Li, Y.H. Jia, Y.L. Li, S.L. Li, X.Y. Fang, M.S. Cao, Comparative  
899 study on transport properties and scattering mechanism of group iii doped sic  
900 nanotube. *Physics letters A* **382**(35), 2484–2488 (2018)  
901  
902  
903  
904 [19] M. Amato, T. Kaewmaraya, A. Zobelli, Extrinsic doping in group iv hexagonal-  
905 diamond-type crystals. *The Journal of Physical Chemistry C* **124**(31), 17290–  
906 17298 (2020)  
907  
908  
909  
910 [20] C.R. Helms, E.H. Poindexter, The silicon-silicon dioxide system: Its microstruc-  
911 ture and imperfections. *Reports on Progress in Physics* **57**(8), 791 (1994)  
912  
913  
914 [21] S. Suthaharan, P. Iyngaran, N. Kuganathan, A. Chroneos, Defects, diffusion  
915 and dopants in the ceramic mineral “lime-feldspar”. *Journal of Asian Ceramic*  
916 *Societies* **9**(2), 570–577 (2021)  
917  
918  
919  
920

- [22] E. Igumbor, E. Omotoso, W.E. Meyer, in *Nano Hybrids and Composites*, vol. 16 (Trans Tech Publ, 2017), pp. 47–51
- [23] E. Igumbor, R.E. Mapasha, W.E. Meyer, Ab-initio study of aluminium impurity and interstitial-substitutional complexes in ge using a hybrid functional (hse). *Journal of Electronic Materials* **46**(7), 3880–3887 (2017)
- [24] J. Adey, R. Jones, D. Palmer, P. Briddon, S. Öberg, Theory of boron-vacancy complexes in silicon. *Physical Review B* **71**(16), 165211 (2005)
- [25] E. Igumbor, G. Dongho-Nguimdo, R.E. Mapasha, W.E. Meyer, Electronic properties and defect levels induced by group iii substitution–interstitial complexes in ge. *Journal of Materials Science* **54**(15), 10798–10808 (2019)
- [26] P. Deák, A. Gali, A. Sólyom, A. Buruzs, T. Frauenheim, Electronic structure of boron-interstitial clusters in silicon. *Journal of Physics: Condensed Matter* **17**(22), S2141 (2005)
- [27] J. Weber, W. Koehl, J. Varley, A. Janotti, B. Buckley, C. Van de Walle, D. Awschalom, Defects in sic for quantum computing. *Journal of Applied Physics* **109**(10), 102417 (2011)
- [28] E. Igumbor, H.T. Danga, E. Omotoso, W.E. Meyer, Defect levels induced by double substitution of b and n in 4h-sic. *Nuclear Instruments and Methods in Physics Research Section B: Beam Interactions with Materials and Atoms* **442**, 41–46 (2019)
- [29] D. Sprouster, C. Campbell, S. Buckman, G. Impellizzeri, E. Napolitani, S. Ruffell, J. Sullivan, Defect complexes in fluorine-implanted germanium. *Journal of Physics D: Applied Physics* **46**(50), 505310 (2013)

- 967 [30] J. Kujala, T. Südkamp, J. Slotte, I. Makkonen, F. Tuomisto, H. Bracht, Vacancy-  
968 donor complexes in highly n-type ge doped with as, p and sb. *Journal of Physics:*  
969 *Condensed Matter* **28**(33), 335801 (2016)  
970  
971  
972  
973 [31] A. Abiona, Palladium-defect complexes in germanium: Experimental and density  
974 functional theory studies of defect pairing in group iv semiconductors. Ph.D.  
975 thesis, UNSW Sydney (2014)  
976  
977  
978 [32] J. Heyd, G.E. Scuseria, M. Ernzerhof, Hybrid functionals based on a screened  
979 coulomb potential. *The Journal of chemical physics* **118**(18), 8207–8215 (2003)  
980  
981  
982 [33] G. Kresse, J. Furthmüller, Efficient iterative schemes for ab initio total-energy  
983 calculations using a plane-wave basis set. *Physical review B* **54**(16), 11169 (1996)  
984  
985  
986 [34] G. Kresse, D. Joubert, From ultrasoft pseudopotentials to the projector  
987 augmented-wave method. *Physical review b* **59**(3), 1758 (1999)  
988  
989  
990 [35] P. Deák, B. Aradi, T. Frauenheim, E. Janzén, A. Gali, Accurate defect levels  
991 obtained from the hse06 range-separated hybrid functional. *Physical Review B*  
992 **81**(15), 153203 (2010)  
993  
994  
995 [36] E. Igumbor, R.C. Andrew, W.E. Meyer, Rare earth interstitials in ge: A hybrid  
996 density functional theory study. *Journal of Electronic Materials* **46**(2), 1022–1029  
997  
998  
999 (2017)  
1000  
1001  
1002 [37] P. Śpiewak, J. Vanhellemont, K. Sueoka, K. Kurzydłowski, I. Romandic, Ab-initio  
1003 simulation of self-interstitial in germanium. *Materials science in semiconductor*  
1004 *processing* **11**(5-6), 328–331 (2008)  
1005  
1006  
1007 [38] H. Tahini, A. Chroneos, R. Grimes, U. Schwingenschlögl, H. Bracht, Diffusion of e  
1008 centers in germanium predicted using gga+ u approach. *Applied Physics Letters*  
1009  
1010  
1011  
1012

|      |  |      |
|------|--|------|
|      | 99(7) (2011)   | 1013 |
|      |  | 1014 |
| [39] | E. Igumbor, K. Obodo, W.E. Meyer, Ab initio study of MgSe self-interstitial (Mgi and Sei). Solid State Phenomena <b>242</b> , 440–446 (2015)   | 1015 |
|      |  | 1016 |
|      |  | 1017 |
|      |  | 1018 |
| [40] | F. Morin, J.P. Maita, Conductivity and hall effect in the intrinsic range of germanium. Physical Review <b>94</b> (6), 1525 (1954)   | 1019 |
|      |  | 1020 |
|      |  | 1021 |
|      |  | 1022 |
|      |  | 1023 |
| [41] | E. Igumbor, O. Olaniyan, G.M. Dongho-Nguimdo, R. Mapasha, S. Ahmad, E. Omotoso, W.E. Meyer, Electronic properties and defect levels induced by n/p-type defect-complexes in ge. Materials Science in Semiconductor Processing <b>150</b> , 106906 (2022) | 1024 |
|      |  | 1025 |
|      |  | 1026 |
|      |  | 1027 |
|      |  | 1028 |
|      |  | 1029 |
|      |  | 1030 |
| [42] | C. Freysoldt, J. Neugebauer, C.G. Van de Walle, Electrostatic interactions between charged defects in supercells. physica status solidi (b) <b>248</b> (5), 1067–1076 (2011)   | 1031 |
|      |  | 1032 |
|      |  | 1033 |
|      |  | 1034 |
|      |  | 1035 |
|      |  | 1036 |
| [43] | E. Igumbor, C. Ouma, G. Webb, W. Meyer, Ab-initio study of germanium di-interstitial using a hybrid functional (HSE). Physica B: Condensed Matter <b>480</b> , 191–195 (2016)  | 1037 |
|      |  | 1038 |
|      |  | 1039 |
|      |  | 1040 |
|      |  | 1041 |
|      |  | 1042 |
| [44] | J.C. Slater, Atomic radii in crystals. The Journal of Chemical Physics <b>41</b> (10), 3199–3204 (1964)  | 1043 |
|      |  | 1044 |
|      |  | 1045 |
|      |  | 1046 |
| [45] | L.C.T. Cao, L. Hakim, S.H. Hsu, in <i>Characteristics and Applications of Boron</i> (IntechOpen, 2022)   | 1047 |
|      |  | 1048 |
|      |  | 1049 |
|      |  | 1050 |
| [46] | K. Choe, M. Hogsed, N. Miguel, J. McClory, J. Kouvetakis, Displacement damage effects in germanium tin leds. Tech. rep., Air Force Institute of Technology Wright-Patterson AFB United States (2020)   | 1051 |
|      |  | 1052 |
|      |  | 1053 |
|      |  | 1054 |
|      |  | 1055 |
|      |  | 1056 |
|      |  | 1057 |
|      |  | 1058 |